A Novel Approach for Wall Shear Rate Estimation based on Bi-Plane Imaging and Sparse Arrays

Giangrossi, Claudio; Pit, Milan; Lopata, Richard; Vos, Hendrik J.; Boni, Enrico; Ramalli, Alessandro

DOI
10.1109/IUS62464.2025.11201756

Publication date
2025

Document Version
Final published version

Published in
2025 IEEE International Ultrasonics Symposium, IUS 2025

A Novel Approach for Wall Shear Rate Estimation based on Bi-Plane Imaging and Sparse Arrays

Claudio Giangrossi[1], Milan Pit[2], Richard Lopata[2], Hendrik J. Vos[3], Enrico Boni[1], Alessandro Ramalli[1]

E-mail: claudio.giangrossi@unifi.it

[1]Department of Information Engineering, University of Florence, Florence, Italy

[2]Department of Biomedical Engineering, Eindhoven University of Technology, PULS/e Lab, Eindhoven, The Netherlands

[3]Department of Imaging Physics, Delft University of Technology, Delft, The Netherlands

2025 IEEE International Ultrasonics Symposium (IUS) | 979-8-3315-2332-9/25/$31.00 ©2025 IEEE | DOI: 10.1109/IUS62464.2025.11201756

***Abstract*— Wall shear rate (WSR), a key marker of vascular health, is useful for cardiovascular risk assessment. Traditionally, its non-invasive evaluation via ultrasound relies on longitudinal imaging of the artery, a method that can be restrictive for comprehensive hemodynamic monitoring. Here a bi-plane ultrasound method using a 2D sparse array for fast, cross-sectional WSR estimation is presented. The technique provides 12 simultaneous, angularly distributed WSR estimates per frame, overcoming limitations of conventional methods and avoiding the hardware complexity of full 3D imaging. Phantom experiments were conducted at different depths with good accuracy (bias < 16%) and repeatability (< 21%).**

Keywords—wall shear rate, bi-plane imaging, sparse arrays, high frame rate color flow mapping, ULA-OP 256.

I. Introduction

Wall shear rate (WSR) is a key hemodynamic parameter that describes the rate at which blood velocity changes near the arterial wall. It is closely related to wall shear stress, a critical factor in evaluating endothelial function. Low wall shear stress is associated with an increased risk of plaque formation, potentially leading to atherosclerosis, while abnormally high in the presence of stenosis may induce plaque rupture, increasing the likelihood of stroke or ischemic events [1], [2], [3], [4], [5], [6]. Hence, the non-invasive monitoring of WSR holds significant clinical value for predicting atherosclerotic risk, evaluating treatment efficacy, and tracking the progression of cardiovascular diseases.

Traditionally, ultrasound-based WSR estimation is limited to longitudinal views of the artery, with velocity measures relying on single-gate [7], multi-gate [8], [9] or at best 2D vector Doppler [10], [11] techniques for velocity measurements. While useful, this approach offers only partial insight, and results can be compromised by probe misalignment. Although 3D methods have been proposed to overcome these limitations, they typically require complex hardware and involve high computational costs, hindering their real-time applicability and thus clinical adoption.

This work presents a novel method that offers a computationally efficient compromise between full 3D imaging and conventional longitudinal views. By exploiting a bi-plane imaging approach with a 2D sparse array, the proposed method enables WSR estimation across the entire cross-section of the artery, offering a new view of hemodynamic forces without the complexity and cost of full 3D imaging.

II. Methods

A. Velocity estimation with bi-plane imaging

The Wall shear rate estimation heavily rely on accurate velocity estimation and precise wall detection. Velocity estimation is here achieved using high-frame-rate color flow mapping (HFR CFM) applied to the artery's cross-sectional view (Fig. 2, panel C), combined with the beam-to-flow angle derived from a wall tracking algorithm (WTA) [12], [13] that identifies wall positions (Fig. 2, panel A). Based on these data, the velocity distribution is computed as

$$v(x,z) = \frac{f_d(x,z)\cdot c}{2f_0 \cdot \cos\vartheta} \tag{1}$$

where f_0 is the transmission frequency, $f_d(x,z)$ is the 2D map of the mean Doppler shifts, ϑ the Doppler angle and c the ultrasound propagation speed.

B. Clutter rejection

Since the velocity distribution near the arterial wall is typically affected by clutter, especially in the region where WSR is calculated, clutter filtering is essential prior to WSR estimation.

The filtering approach used in this work was originally proposed by *Ricci et al*. [9] for single-line velocity estimation in longitudinal views, and it is based on reconstructing the velocity profile using a power-law fitting model.

In this study, the method is extended to cross-sectional data and works as follows:

The WTA identifies the coordinates of 90 points along the vessel walls in the cross-sectional view, as previously presented in [14]. These coordinates serve as spatial reference to mask the velocity profile within the flow region. To mitigate inaccuracies commonly observed near the vessel boundaries, the outermost 15% of the flow area, delimited by the blue dotted line in Fig. 1, is excluded for the estimation. Consequently, the region of interest is confined to the innermost 85%, where velocity

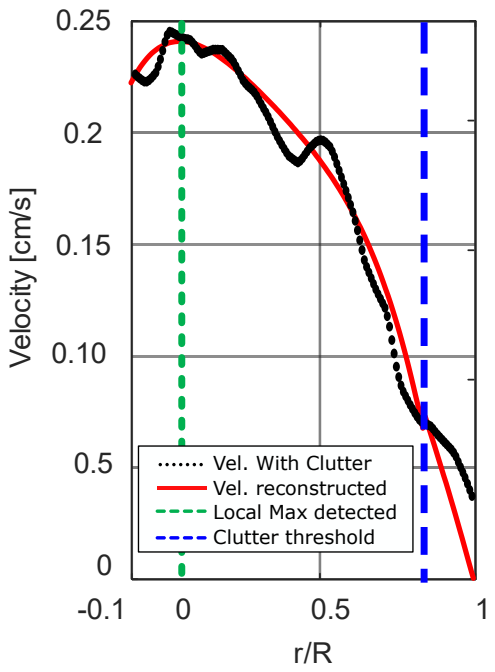

Fig. 1 The graph shows the original velocity profile in black and the reconstructed velocity profile in red. The dashed blue line shows the clutter region threshold and the green one the detected local maximum.

estimates are more reliable. This flow region is then used for fitting a power-law model, defined as follows:

$$v(r,\alpha) = a \cdot \left(1 - \left|\frac{r-b}{R_w-b}\right|^n\right) \quad (2)$$

The velocity distribution, initially expressed in Cartesian coordinates (x, z) in Eq. 1 is transformed into polar coordinates (r, α) centered on the vessel central axis, where r represents the radial distance from the center and α the angular position around the perimetral wall, R_w the distance of the wall detected by the WTA, a is the peak velocity at the local maximum, b is the abscissa of the symmetry axis, and n is the exponent that best fits the velocity profile. For example, n = 2 corresponds to a parabolic profile.

In detail, the algorithm searches for local maxima (Fig. 1, green dotted lines) in the velocity profile, allowing for the presence of physiological M-shaped profiles. Since the measured velocity often does not drop to zero (see Fig. 1, black dots) at the wall due to clutter noise and sample volume size, the model constrains the velocity to be zero at the vessel boundary. The optimal power-law exponent n is then obtained by fitting the modeled profile to the measured data, subject to the boundary condition at the wall. After reconstructing the velocity profile along a single radial direction defined by an angle α (see Fig. 1, red line), this procedure is iteratively repeated for all angular positions α covering the whole vessel

C. *Wall shear rate estimation*

To estimate the WSR along the entire arterial wall, the WTA is applied to the cross-sectional view to localize the vessel walls (Fig. 2, panel B). The shear rate is then computed slicing radially the velocity gradient at the wall detected by the WTA R_w as follows:

$$WSR(\alpha) = \frac{dv(r,\alpha)}{dr}\Big|_{r=R_w} \quad \alpha \in [0,2\pi) \quad (3)$$

The HFR and WTA are performed in real-time (Fig. 2, panels A, B and C), while the WSR computation is performed in post-processing through a MATLAB script. Finally, for each elaborated frame, calculated WSR are averaged and shown over 12 evenly distributed, 30°-wide arcs across the vessel (Fig. 2, panel D) , as this segmentation offers a practical and sufficiently detailed representation of the WSR distribution while preserving clarity and interpretability.

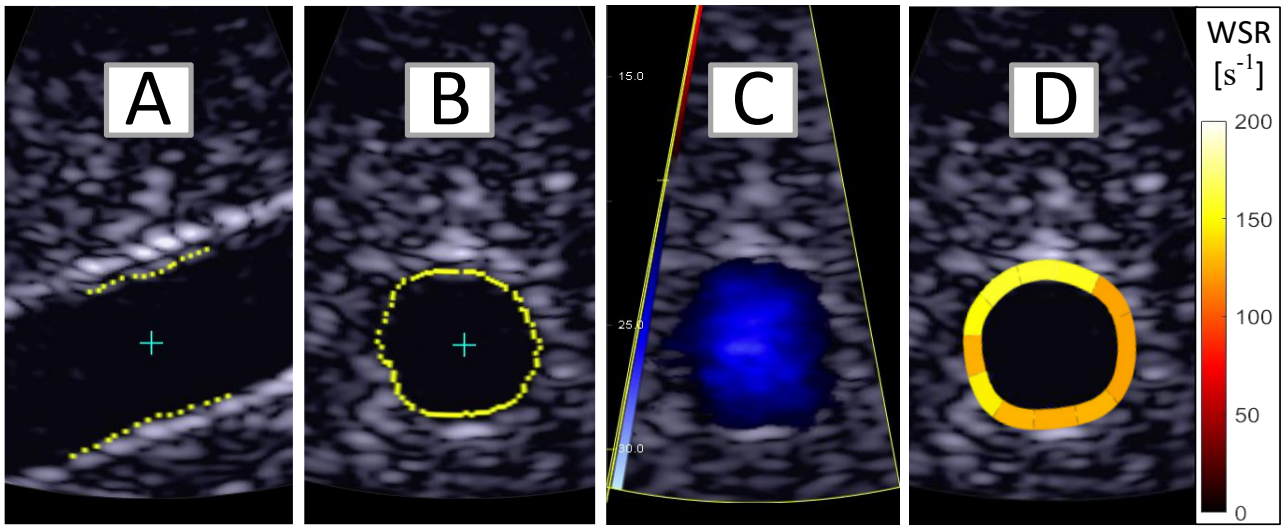

Fig. 2 The ULA-OP 256 real-time interface for wall tracking algorithm in the longitudinal view (panel A) and cross-sectional view (panel B), the HFR CFM in the cross section (panel C), and the instantaneous WSR estimated in post-processing across the 12 sectors (panel D).

D. Experimental setup

The probe used for bi-plane imaging was a 5 MHz, 256-element 2D spiral array prototype [15], developed by TU Delft (the Netherlands). Each transducer element is independently connected to a channel of the ULA-OP 256 research scanner [16]. The scanner was programmed to interleave the transmissions of diverging waves, covering a 72-line sector, for HFR-CFM on the cross-sectional view, and focused transmissions for the two 96-line B-mode planes used for wall tracking. The PRF was set to 3.6 kHz, corresponding to 1800 frames per second input to the HFR CFM processing module. Validation was conducted through acquisitions on a hydraulic circuit comprising a peristaltic pump that circulated a blood-mimicking fluid through a 7 mm-diameter vessel phantom, and a flow sensor used as reference.

E. Phantom tests

The tests were conducted under steady flow conditions at three different flow rates (100, 200, 300 ml/min) and two different vessel depths (20, 40 mm). The probe was positioned over the phantom to maintain a 60° Doppler angle. For each setting, ten 6-second acquisitions were processed. The 12 estimations from all frames were then used to calculate the mean bias and its standard deviation. An ideal parabolic steady flow WSR for a 7 mm vessel and the corresponding relative flow volume were used as the WSR ground truth.

III. Results and Discussion

Fig. 3 illustrates the temporal trend of the WSR for one of the 12 evenly distributed segments during a sample test. Ideally, the WSR should be represented by a steady line without fluctuations. However, the observed oscillations in the estimated WSR could be due to measurement errors as well as potential flow disturbances introduced by the peristaltic pump used in the experimental setup. Despite these fluctuations, the estimated WSR remains closely centered around ground truth values. The quantitative results are shown in Table I. The

TABLE I. Mean bias and SD of phantom tests

	Flow volume [ml/min]	Expected WSR [s^{-1}]	Bias [%]	SD [%]
Vessel depth 20 mm	100	49	+10.6%	12.8%
	200	99	+3.0%	16.0%
	300	148	-1.6 %	17.6 %
Vessel depth 40 mm	100	49	+15.5%	15.4%
	200	99	+9.48%	18.8%
	300	148	+10.2 %	21 %

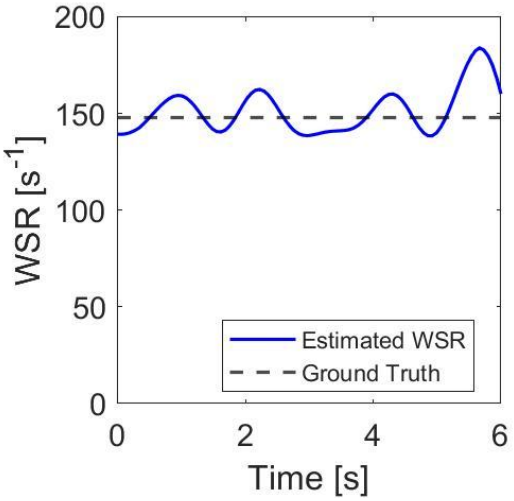

Fig. 3 Sample temporal trend of the WSR estimation in one of the 12 sectors during a phantom acquisition.

method achieves higher accuracy at a depth of 20 mm, with a mean bias consistently below 11% across all tested flow rates. The best performance is observed at higher flow rates. Repeatability remains below 18%, a level comparable to that reported by other methods in the literature. At increased depths of measurement, such as 40 mm, the mean bias in WSR estimation shows a modest increase up to approximately 15.5%, while repeatability slightly declines but remains below 21%, confirming the method's accuracy and stability over time.

IV. Conclusions

This work presented a novel method for estimating Wall Shear Rate directly from cross-sectional ultrasound images of the vessel. Using bi-plane imaging with a spiral probe, 12 instantaneous radial measurements are obtained and evenly distributed along the arterial perimeter, providing valuable hemodynamic information. Although full 3D techniques offer detailed volumetric data, they often require complex hardware and extensive post-processing, which limits their applicability in real-time settings. Although not suitable for highly turbulent flow conditions, the method is appropriate for diagnostic assessment of large vessels and bridges the gap to real-time processing while facilitating integration with ultrasound systems for potential clinical applications. Future work will focus on validating the method under physiologically pulsatile flow conditions to capture dynamic WSR variations, as well as conducting in vivo tests to assess its clinical relevance and robustness.

Acknowledgment

This work was supported by PRIN 2020 project CONUS (CUP: B13C21000190005) under Grant 20205HFXE7, funded by the Italian Ministry of Education, University and Research.

References

[1] P. Eshtehardi *et al.*, "High wall shear stress and high-risk plaque: an emerging concept," *Int J Cardiovasc Imaging*, vol. 33, no. 7, pp. 1089–1099, Jul. 2017, doi: 10.1007/s10554-016-1055-1.

[2] G. C. Makris, A. N. Nicolaides, X. Y. Xu, and G. Geroulakos, "Introduction to the biomechanics of carotid plaque pathogenesis and rupture: review of the clinical evidence," *British Journal of Radiology*, vol. 83, no. 993, pp. 729–735, Sep. 2010, doi: 10.1259/bjr/49957752.
[3] S. S. Dhawan *et al.*, "Shear stress and plaque development," *Expert Review of Cardiovascular Therapy*, vol. 8, no. 4, pp. 545–556, Apr. 2010, doi: 10.1586/erc.10.28.
[4] C. J. Slager *et al.*, "The role of shear stress in the generation of rupture-prone vulnerable plaques," *Nat Rev Cardiol*, vol. 2, no. 8, pp. 401–407, Aug. 2005, doi: 10.1038/ncpcardio0274.
[5] K. C. Koskinas, Y. S. Chatzizisis, A. B. Baker, E. R. Edelman, P. H. Stone, and C. L. Feldman, "The role of low endothelial shear stress in the conversion of atherosclerotic lesions from stable to unstable plaque," *Current Opinion in Cardiology*, vol. 24, no. 6, p. 580, Nov. 2009, doi: 10.1097/HCO.0b013e328331630b.
[6] S.-K. Jeong, J.-Y. Lee, and R. S. Rosenson, "Association between Ischemic Stroke and Vascular Shear Stress in the Carotid Artery," *Journal of Clinical Neurology*, vol. 10, no. 2, pp. 133–139, Apr. 2014, doi: 10.3988/jcn.2014.10.2.133.
[7] J. R. Blake, S. Meagher, K. H. Fraser, W. J. Easson, and P. R. Hoskins, "A Method to Estimate Wall Shear Rate with a Clinical Ultrasound Scanner," *Ultrasound in Medicine & Biology*, vol. 34, no. 5, pp. 760–774, May 2008, doi: 10.1016/j.ultrasmedbio.2007.11.003.
[8] P. J. Brands, A. P. G. Hoeks, L. Hofstra, and R. S. Reneman, "A noninvasive method to estimate wall shear rate using ultrasound," *Ultrasound in Medicine & Biology*, vol. 21, no. 2, pp. 171–185, Jan. 1995, doi: 10.1016/S0301-5629(94)00111-1.
[9] S. Ricci, A. Swillens, A. Ramalli, P. Segers, and P. Tortoli, "Wall Shear Rate Measurement: Validation of a New Method Through Multiphysics Simulations," *IEEE Transactions on Ultrasonics, Ferroelectrics, and Frequency Control*, vol. 64, no. 1, pp. 66–77, Jan. 2017, doi: 10.1109/TUFFC.2016.2608442.
[10] Y. Du *et al.*, "Wall Shear Stress Measurements Based on Ultrasound Vector Flow Imaging," *Journal of Ultrasound in Medicine*, vol. 39, no. 8, pp. 1649–1664, 2020, doi: 10.1002/jum.15253.
[11] A. J. Y. Chee, C. K. Ho, B. Y. S. Yiu, and A. C. H. Yu, "Time-Resolved Wall Shear Rate Mapping Using High-Frame-Rate Ultrasound Imaging," *IEEE Transactions on Ultrasonics, Ferroelectrics, and Frequency Control*, vol. 69, no. 12, pp. 3367–3381, Dec. 2022, doi: 10.1109/TUFFC.2022.3220560.
[12] M. Demi, M. Paterni, and A. Benassi, "The First Absolute Central Moment in Low-Level Image Processing," *Computer Vision and Image Understanding*, vol. 80, no. 1, pp. 57–87, Oct. 2000, doi: 10.1006/cviu.2000.0861.
[13] V. Gemignani, F. Faita, L. Ghiadoni, E. Poggianti, and M. Demi, "A System for Real-Time Measurement of the Brachial Artery Diameter in B-Mode Ultrasound Images," *IEEE Transactions on Medical Imaging*, vol. 26, no. 3, pp. 393–404, Mar. 2007, doi: 10.1109/TMI.2006.891477.
[14] C. Giangrossi *et al.*, "Blood-flow Volume Estimation by a 2-D Sparse Array," *Ultrasound in Medicine & Biology*, Jul. 2025, doi: 10.1016/j.ultrasmedbio.2025.06.005.
[15] L. Wei *et al.*, "Sparse 2-D PZT-on-PCB Arrays With Density Tapering," *IEEE Transactions on Ultrasonics, Ferroelectrics, and Frequency Control*, vol. 69, no. 10, pp. 2798–2809, Oct. 2022, doi: 10.1109/TUFFC.2022.3204118.
[16] E. Boni *et al.*, "ULA-OP 256: A 256-Channel Open Scanner for Development and Real-Time Implementation of New Ultrasound Methods," *IEEE Transactions on Ultrasonics, Ferroelectrics, and Frequency Control*, vol. 63, no. 10, pp. 1488–1495, Oct. 2016, doi: 10.1109/TUFFC.2016.2566920.